Journal of Energy and Power Engineering 12 (2018) 517-532
doi: 10.17265/1934-8975/2018.11.002

Molten Salts and Applications II: 565 °C Molten Salt Solar Energy Storage Design, Corrosion, and Insulation

Samaan Ladkany, William Culbreth and Nathan Loyd

Howard Hughes College of Engineering, University of Nevada, Las Vegas, Las Vegas, NV 89154, USA

Abstract: Excess energy from various sources can be stored in molten salts (MS) in the 565 °C range. Large containers can be used to store energy at excess temperatures in order to generate eight hours or more of electricity, depending on the container size, to be used during peak demand hours or at night for up to a week. Energy storage allows for a stable diurnal energy supply and can reduce the fluctuation due to weather conditions experienced at thermal solar power stations. Supported by Office of Naval Research (ONR), this paper discusses the design considerations for molten salt storage tanks. An optimal molten salt storage tank design layout is presented, as well as alternative designs for the storage tanks. In addition, the costs and corrosion effects of various molten salts are discussed in order to show the effects these considerations have on the design process.

Key words: Molten salt storage tank design, molten salt technology, molten salt properties, molten salt costs, solar energy storage, nuclear energy storage.

1. Introduction

Molten solar salts have considerable capacities for heat storage, which makes them effective at storing excess energy. Large insulted tanks provide a closed system for these molten salts to be properly contained. This paper examines important tank design considerations, the layout of an optimal tank design, and alternative design proposals. This paper also examines the costs, and corrosion properties of various molten salts. The material presented in this paper has been collected by the researchers in the University of Nevada, Las Vegas (UNLV) Molten Salt Project and information provided in a report to the project [1, 2].

This paper is the second paper of a three part series on Molten Salt Research, with the previous paper being "Molten Salt History, Types, Thermodynamic and Physical Properties, and Cost" [3] and the following paper being "Worldwide Molten Salt Technology Developments in Energy Production and Storage" [4].

Corresponding author: Dr. Craig Tyner, Ph.D. in Chemical Engineering, consultant and former CEO of Halotechnics, research fields: concentrating solar power and molten salts.

2. Optimal Design of Molten Salt Storage Tanks

Gabrielli and Zamparelli [5] present an optimal design for molten salt storage tanks. Based on their process, the first step was determining the height and diameter of the tank, followed by the determination of the thicknesses of all shell layers that best limit heat loss. After this information has been determined, a finite element model (FEM) analysis is performed to check the structural design, and then a cost analysis is performed to determine if the design is economical.

Based on this procedure, the resulting design is a cylindrical storage tank with a SA-516 Grade 70 carbon steel shell, used for both the cylindrical shell and the roof shell, as shown in Fig. 1. Outside the carbon steel shell is a layer of ceramic insulation. Inside the cylindrical carbon steel shell, there is a layer of firebrick insulation. Directly above the firebrick insulation is a plate of ceramic insulation supported from the tank roof that prevents heat from reaching the roof shell. Lastly, there is a flexible layer of AISI 321H stainless steel inside of the firebrick insulation and the top ceramic insulation which is

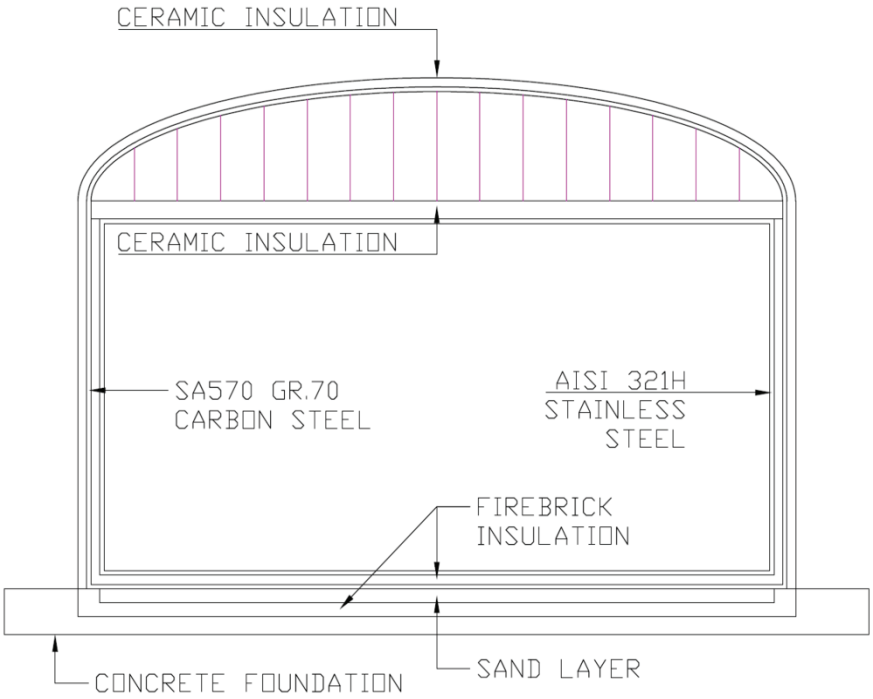

Fig. 1 Optimal tank design layout [5].

used to provide corrosion resistance. Based on their design process, the height of the tank should not exceed 12 meters (39.37 feet) because that is the maximum length of piping that the pumps allow based on what is commercially available [5]. Two alternative tank designs, neither of which use firebrick insulation, are presented later in this paper, one with a carbon steel structural shell and one with a concrete structural shell.

3. Corrosion from Molten Salts

Molten salts are also known for their corrosive nature as much as their ability to store heat. The corrosion properties of stainless steel exposed to various molten salts are presented in Table 1.

At a temperature of 565 °C, the solar salt mixture corrodes the SS 316 stainless steel at 0.05 millimeters per year [6]. At 845 °C, sodium chloride corrodes both types of stainless steel at 7.2 millimeters per year [7]. In addition to being highly corrosive, sodium chloride is also dangerous in case of decomposition. Hitec Salt corrodes at 538 °C through SS 304 steel at 0.21 millimeters per year, and through the SS 316 steel at less than 0.03 millimeters per year [7]. Lastly, Hitec Salt corrodes at 430 °C through SS 316 steel 0.007 millimeters per year, 0.008 millimeters per year at 505 °C, and 0.074 millimeters per year at 550 °C [7].

Although nitrate salts are strong oxidizers, they are generally easily contained with conventional materials. At temperatures up to about 400 ºC, inexpensive carbon steels are used for cold salt piping, cold tanks, and hot tanks in trough applications. Above 400 ºC, most 300-series stainless steels (e.g., 304, 316, 347) and high nickel alloys (e.g., Inconel 625 and Haynes

Table 1 Corrosion properties of stainless steel using molten salts [6, 7].

Compound or mixture	Temperature (°C)	Corrosion rate (mm/y)	
		SS 304	SS 316
Solar salt (60:40 Na:K nitrate by weight)	580	------	0.05
Sodium chloride—NaCl	845	7.2	7.2
Hitec salt (7:53:40 $NaNO_3$:KNO_3:$NaNO_2$ by weight)	538	0.21	< 0.03
	430	------	0.007
	505	------	0.008
	550	------	0.074

230) have very low corrosion rates in contact with hot salt and are acceptable for containment materials (even for the very thin-walled (~1 mm) receiver tubes). Hot storage tanks for power tower applications are generally fabricated from one of the 300-series stainless steels.

Industrial grade nitrate materials can be mined and purified, or synthetically produced, which is typical for KNO_3. Salt purity is specified in terms of allowable contaminant levels, with chloride and $Mg(NO_3)_2$ levels typically most important. High chloride levels can lead to accelerated corrosion, while $Mg(NO_3)_2$ decomposes on initial heating to hot salt temperature, releasing NO_2, an environmental and personnel hazard during plant start-up.

Salt specification and as-received impurity levels for Solar Two are shown in Table 2 and Fig. 2 [8].

This material proved completely satisfactory, except for the magnesium content, which resulted in NO_2 evolution during initial heat-up of the salt inventory to hot salt temperatures. Once the initial heat-up was complete and all $Mg(NO_3)_2$ converted to MgO (which precipitated out, presenting no further problems), NO_2 evolution stopped and no other issues were observed.

A current typical impurity specification for solar salt is shown below in Table 3. 60/40 Na/KNO_3 must be at least 98%. Note that the magnesium specification is much tighter since the Solar Two experience.

As discussed above, nitrate and nitrite materials are compatible with common steels and stainless steels at typical solar operating conditions, and thus not a problem. Chlorides and other potentially higher temperature materials would have to be very carefully evaluated and tested to assure compatibility [9]. While some ceramics have potential as containment materials, ceramic brittleness and lack of simple connection approaches (like welding for metals) make their use problematic. While some ceramics have potential as containment materials, ceramic brittleness and lack of simple connection approaches make their use problematic. The authors are considering the use of high temperature and refractory concretes as isolators and insulation materials between a stainless steel inner container and an outside supporting structures.

Table 2 Solar two salt as-received impurity levels [8].

Impurity	Concentration [%]
Magnesium	0.045
Chloride	0.36
Perchlorate	0.26
Carbonate	0.00234
Hydroxide	0.00
Sulfate	0.12
Nitrite	0.00
Chromium	0.00

Table 3 Typical solar salt specification by weight [9].

Impurity	Maximum allowable [%]
Total Chloride	0.60%
Perchlorate	0.25%
Magnesium	0.005%
Nitrite	1.00%
Sulfate	0.75%
Carbonate	0.10%
Hydroxyl	0.20%
Any other impurities	< 0.04%

- 3.37 million pounds of nitrate salt prills with a nominal composition, by weight, of 60 percent $NaNO_3$ and 40 percent KNO_3, which was delivered in 2,200 lb (1,000 kg) bags. The minimum acceptable nitrate salt concentration was 98 percent by weight.
- Maximum chloride ion concentration, from all sources, is 0.6 percent by weight.
- Maximum contamination, by weight, from other, non-chloride sources, as follows:
  - Nitrite—1.00 percent
  - Carbonate—0.10 percent
  - Sulfate—0.75 percent
  - Hydroxyl alkalinity—0.20 percent
- Notification to the buyer if the concentration of any unnamed species exceeded 0.10 percent by weight.

Fig. 2 Optimal tank design layout criteria [5].

4. Molten Salt Insulation

Insulation and heat trace techniques were initially developed by Sandia during testing at the NSTTF in the 1980s, and were first employed on a large scale at Solar Two. Heat tracing is typically done with mineral insulated (MI) cable (similar to the heating element in a kitchen oven) strapped to bare pipe, instrumented with thermocouples for control purposes, and covered with a stainless steel foil to prevent subsequent layers of insulation from getting between the cable and the pipe. Computer control maintains the piping at desired temperatures (depending on pipe size, but always near or above salt freezing temperatures). Heat trace control zones vary in size from single zones on long piping runs to individual control zones on every valve.

Insulation is relatively standard, with a soft batt insulation wrapped around the pipe and then typically covered with a rigid calcium silicate-type industrial insulation. An outer layer of aluminum lagging is used to protect the insulation from the weather. In addition to preventing freezing and minimizing heat loss, the insulation must be adequate to keep surface temperatures within OSHA requirements for personnel safety.

The MS storage tanks themselves are similarly insulated externally with flexible batt insulation and lagging. Internal heaters are used to prevent freezing of salt in the tanks during extended outages (although generally the tanks are so large that they can go weeks, if not months, without dropping to salt freezing temperatures during an outage).

When properly installed, insulation and heat tracing function as intended and are not significant performance or maintenance issues. However, extreme care must be taken to assure installation to exacting specifications, otherwise problems resulting in local overheating and pipe corrosion caused by excessively high local temperatures may result. Poor insulation techniques can cause gaps, which can result in freezing, especially in smaller pipes and tubing.

Some ternary mixtures have melting points between 100 and 200 ºC, which would lessen the issues associated with salt freezing, but not eliminate them. Heat tracing and insulation would still be required, although lesser standards could perhaps be applied. It is notable that future research may involve ternary salt mixtures, which could be used to lower the melting point or the high temperature in the 700 ºC or higher and allowing for more efficient plant operations. Synthetic oils used as trough working fluid freeze at temperatures only slightly above ambient; heat tracing is not generally required, although oil must be circulated through receiver and field piping elements during non-solar hours to prevent freezing.

Note that salt freezing is one of the main issues with use of salt as the working fluid in troughs or CLFRs. Extremely long field piping runs, particularly of exposed receiver tubing, are very difficult to either drain or prevent from freezing [2].

5. Structural Design Methods for Steel MS Storage Tanks

Typically, cylindrical shells of a hybrid of carbon and stainless steels are used to make molten salt (MS) storage tanks. The A588 Carbon Steel serves as an outer structural layer and the 316 Stainless Steel inner layer serves to protect against corrosion. The thickness for the stainless steel from 0.06 inch (1.52 mm) for a 30-year plant life span to 0.10 inch (2.54 mm) for a 50-year plant life span [10]. As a factor of safety, 0.25 inches (6.35 mm) will be used as the design thickness of stainless steel.

6. Tank Requirements

In developing a design for the steel cylindrical tanks, the amount of energy storage must be calculated in order to determine the proper size of the tanks. Research performed by Loyd [10] shows the energy storage calculations for the tanks.

For this stage of the project research, the tanks need to store enough molten solar salt, which is a 60:40

sodium nitrate ($NaNO_3$) and potassium nitrate (KNO_3) mix, to provide power for a 300 megawatt power plant for eight hours each night. Calculations determined that in order to satisfy these requirements, the two tanks need to be able to store 12,048 cubic meters (425.5 × 10^3 ft^3).

In order to determine the total mass of salt required to operate the power plant, the basic energy equation, shown in Eq. (1) [11] is used.

$$E = P_{thermal} * \Delta t_{storage} = m * c_p * \Delta T \quad (1)$$

In Eq. (1) above, E represents the total energy in the system. The power generated by the power plant is $P_{thermal}$, which as stated earlier is 300 megawatts. The required time of storage is $\Delta t_{storage}$, which is 8 hours or 28,800 seconds. The required amount of solar salt needed for the power plant is represented by m. The specific heat capacity of the salt is c_p, which is 1,540 Joules per kilogram of salt per degree kelvin. The temperature range of the salt in the system is ΔT, which is calculated using Eq. (2).

$$\Delta T = T_{salt,max} - (T_{sat} - 20\ K) \quad (2)$$

In Eq. (2) above, the maximum temperature of salt in the system, or $T_{salt,max}$, is 853.15 degrees kelvin. The temperature of the Rankine cycle, T_{sat}, is 620.55 degrees kelvin. Eq. (2) determined that the temperature range for the salt is 252.6 degrees Kelvin.

In order to determine the required mass of salt, Eq. (1) is rearranged into Eq. (3) as shown.

$$m = \frac{P_{thermal} * \Delta t_{storage}}{c_p * \Delta T} \quad (3)$$

This determined that the power plant requires 22.88 × 10^6 kilograms of salt, or 50.44 × 10^6 pounds (25,220 tons).

Eq. (4) is used to determine the volume of solid salt required.

$$V_{salt} = \frac{m}{\rho_{salt}} \quad (4)$$

Equation 4 determined that the volume of solid salt required is 12,048 cubic meters of salt, or 425.5 × 10^3 cubic feet. This volume will be divided over two tanks, requiring 212.7 × 10^3 cubic feet (6,024 cubic meters) for each tank. However, a third and fourth tanks, all of carbon steel, are recommended for the storage of cooled MS after power generation and for safety and continued operations during maintenance of the other tanks.

All structural steel used is A588 Grade 50 steel. The cylindrical tank designed with a 40 feet (12.192 meters) radius at the base. This results in a height of salt of 42 feet (12.802 meters) and a height of 54 feet (16.594 meters) for the cylindrical tank.

7. Cylindrical Tank Structural Designs

The design of a steel shell tank was performed. In performing the structural design for the cylindrical tank, the tank is divided into five different elements. The five elements for the tank design are the shell wall, the top cover which includes a central 10 feet (3.048 meters) diameter steel access dome, steel support columns, a steel bottom, and the concrete slab underneath a layer of sand. The top cover is designed using carbon steel.

In designing the steel tank, the first step is to design the steel shell wall. Under shell theory, axial bending in a cylindrical shell occurs mainly at the base of the shell wall where the base and the shell wall intersect, before bending dissipates further up the wall [12]. An analysis using shell theory determined that axial bending dissipates nine feet (2.374 meters) above ground in the steel shell wall. The first step was to determine the bending in the steel shell wall as shown in Fig. 3 for the steel wall. For the steel wall, the maximum positive axial bending moment is 4.085 kip-foot/foot (18.17 kN·m/m) at the bottom of the shell, and the maximum negative bending moment is 886.2 pound-foot/foot (3.942 kN·m/m) at a height 2.7 feet (826 mm) above the bottom of the shell [10]. Circumferential moments are equal to the Poisson ratio multiplied by the axial moments. For the steel shell wall, the maximum circumferential force occurs at the bottom of the shell wall. In the steel wall, the maximum circumferential force is 177.6 kips per linear foot (klf), which is 2,593 kN/m.

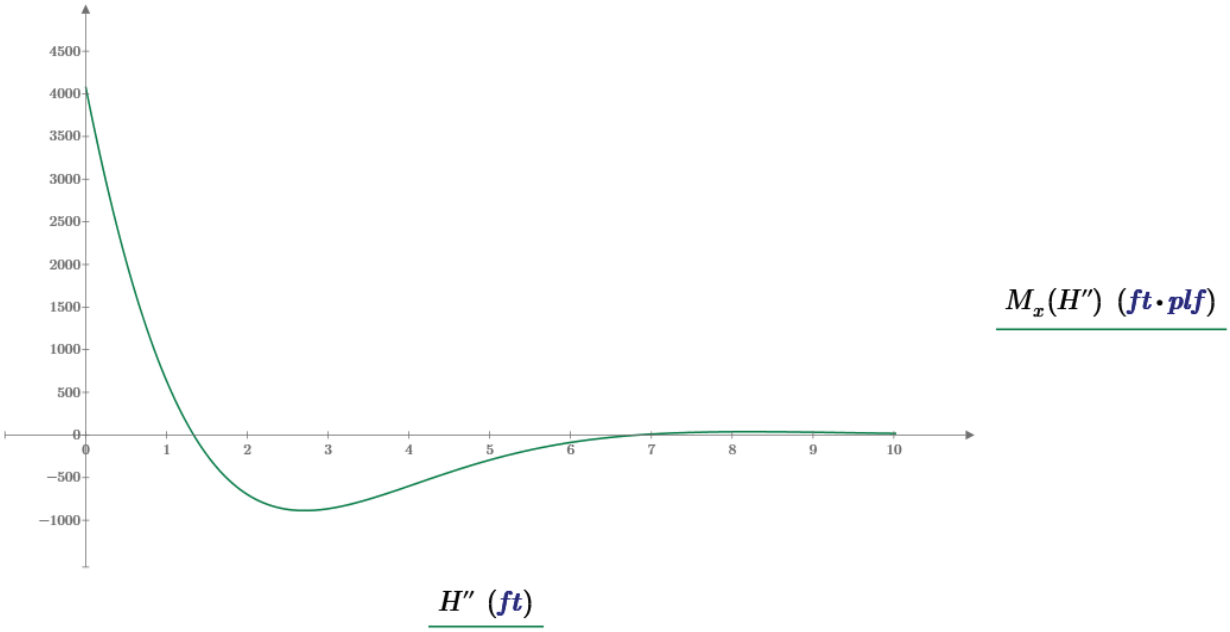

Fig. 3 Steel cylindrical shell wall M_x bending moment [10].

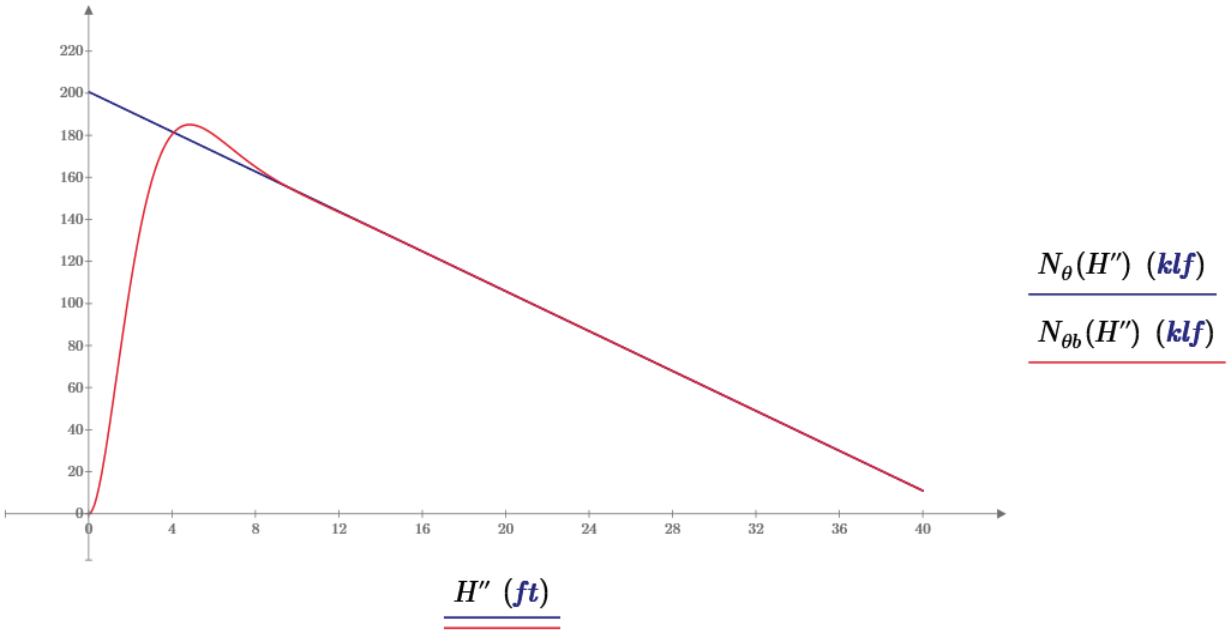

Fig. 4 Steel cylindrical shell wall N_θ forces [10].

The red curve is based on Bending Theory while the blue curve is based on Shell Theory.

Tensile membrane force is determined by Eq. (6) and shown in Fig. 4 for the steel shell wall. The circumferential and axial stresses in the steel wall are shown in Fig. 5 [12].

The maximum axial compressive force, N_x, in the wall at the bottom of the shell is equal to the total dead weight of the shell, top slab, and service dome, plus the total live load, which is the total weight (W), divided by the circumference of the shell [12].

Based on research performed by Nathan Loyd [10], Eqs. (5)-(14) are as follows:

$$p = \gamma z \tag{5}$$

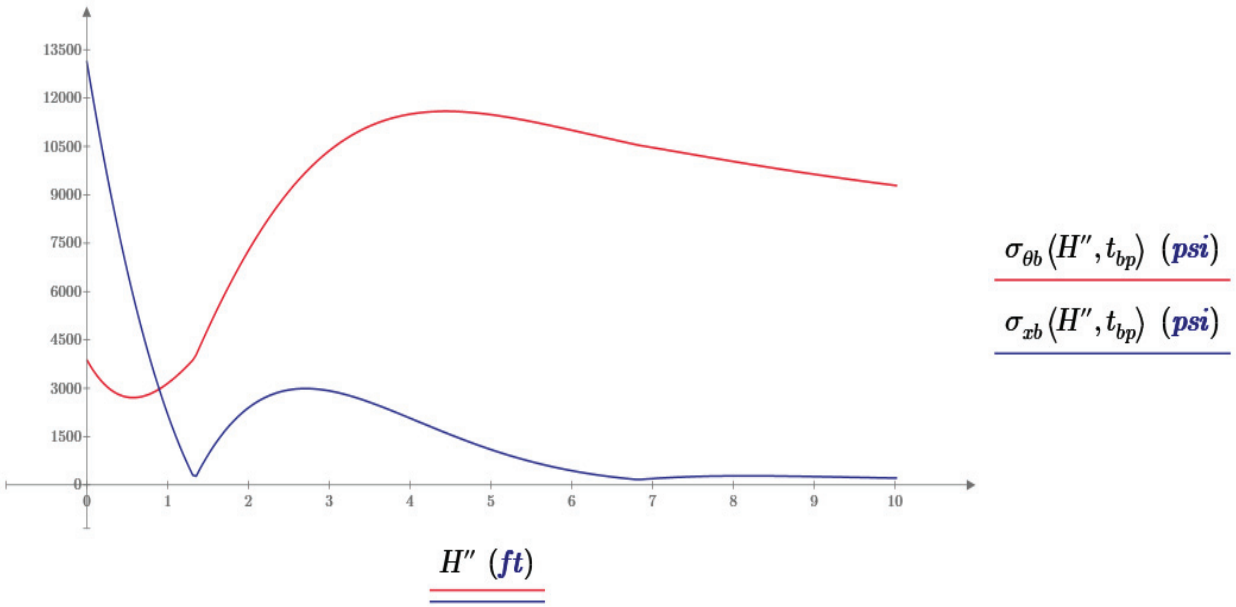

Fig. 5 Stresses at the bottom of the steel shell wall [10].
The red curve is the Circumferential Stress and the blue curve is the Axial Stress.

$$N_\theta = pr \tag{6}$$

$$D = \frac{Et}{12(1-\nu)} \tag{7}$$

$$\beta = \sqrt{\frac{\sqrt{1-\nu^2}}{rt}} \tag{8}$$

$$C_1 = \frac{\gamma h r^2}{Et} \tag{9}$$

$$C_2 = \frac{\gamma r^2}{Et}\left(h - \frac{1}{\beta}\right) \tag{10}$$

$$w = e^{-\beta x}(C_1 \cos \beta x + C_2 \sin \beta x) + \frac{\gamma(h-x)r^2}{Et} \tag{11}$$

$$M_x = D\frac{d^2 w}{dx^2} \tag{12}$$

$$M_\theta = \nu M_x \tag{13}$$

$$N_x = \frac{W_x}{C} \tag{14}$$

In determining the applied pressure on the tank from Eq. (5), it is the product of the salt unit weight (γ) and the depth of salt (z) at the specified point. In Eq. (6), p is the applied pressure on the wall and r is the radius of the wall [12]. In Eqs. (7)-(12), D, β, C_1, and C_2 are coefficients, E is the Young's Modulus of the shell material, t is thickness of the shell wall, ν is the Poisson's ratio of the shell material, h is the total height of molten salt, w is shell wall deflection at a height of x above ground, and the second derivative of w is used to determine the moment at that point [12]. M_x is the axial moment at a height of x above ground, W_x is the weight of the shell including dead and live loads on its top at level above x [12].

Fig. 6 details the design of the steel cylindrical shell and the top dome and Fig. 7 presents a steel cylindrical tank design with an alternative roof shell. The thickness of the steel shell wall is varied to accommodate the loading. At the bottom of the tank, where there are combined bending and axial forces, the bottom nine feet (2.734 meters) of the shell requires a structural steel thickness of 1.5 inches (38.1 mm). The section of the shell wall that is between 9 and 15 feet (2.734 and 4.572 meters) above the ground requires a structural steel thickness of 0.625 inches (15.9 mm). The section of the shell wall that is between 15 and 22 feet (4.572 and 6.706 meters) above the ground requires a structural steel thickness of 0.5 inches (12.7 mm). The

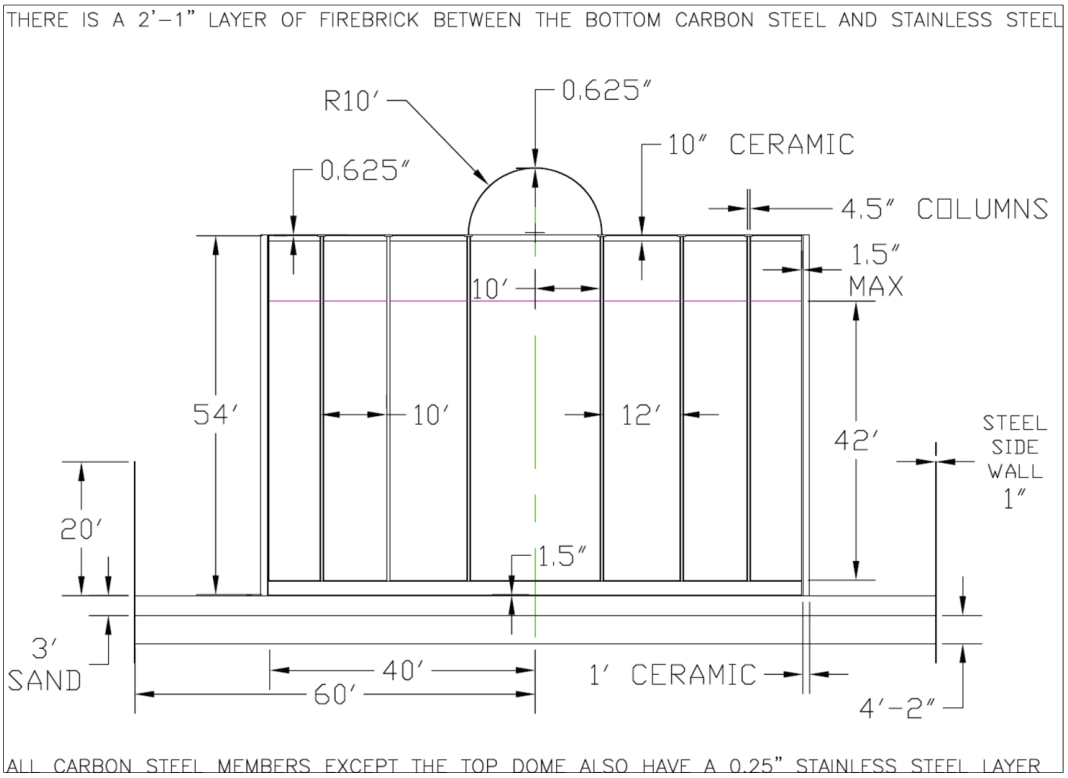

Fig. 6 Steel cylindrical shell model design including top dome, supporting rows of columns, sand layer, 50" posttension slab, and safety steel walls at the edge and excluding the outer layer of insulation [10].

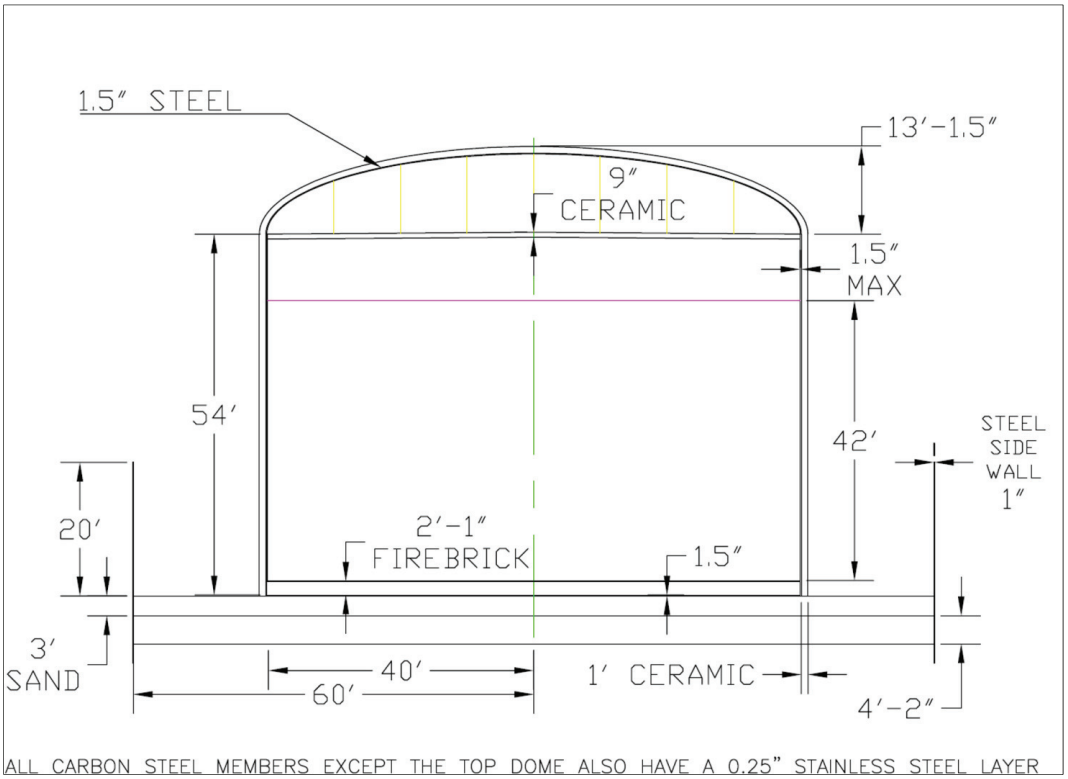

Fig. 7 Steel cylindrical shell model design including alternative elliptical top dome, sand layer, 50" posttension slab, and safety steel walls at the edge and excluding the outer layer of insulation [10].

section of the shell wall that is between 22 and 29 feet (6.706 and 8.839 meters) above the ground requires a structural steel thickness of 0.375 inches (9.5 mm). The section of the shell wall that is between 29 and 36 feet (8.839 and 10.973 meters) above the ground requires a structural steel thickness of 0.25 inches (6.4 mm). All sections of the shell wall above 36 feet (10.973 m) will require a structural steel thickness of 0.125 inches (3.2 mm). Lastly, in order to combat corrosion effects, a 316 Stainless Steel liner of 0.25 inch (6.35 mm) thickness will line the inside of the shell wall [10].

After designing the shell wall, the next design elements for the cylindrical tank were the top plate and the columns that support the plate. The steel shell design uses carbon steel to design the top plate while the concrete shell design uses a concrete top plate. Three circular rows of carbon steel columns, with stainless steel lining, support the top plate. In designing the columns, an extra factor of safety had to be included due to the high temperatures associated with molten salts, which will reach temperatures as high as 565 degrees Celsius. At this temperature, the yield strength of the steel is approximately 60% of its nominal yield strength [13]. The first two rows each contain eight equally spaced columns, with the two rows located ten feet (3.048 meters) and 22 feet (6.706 meters) on center from the center of the tank, respectively. The location of the first row occurs where the 0.625 inch (15.9 mm) thick service dome intersects the top plate of the tank. The final row of columns contains 16 equally spaced columns, which are located 32 feet (9.754 meters) on center from the center of the tank. The steel top plate has a design thickness of 0.625 inches (15.9 mm). The resulting design loads for the columns supporting the steel top plate are 6.5 kips (28.9 kN) for each first row column, 19.6 kips (87.2 kN) for second row columns, and 11.7 kips (52.0 kN) for third row columns.

Based on the AISC Steel Construction Manual [14], the first row columns will be HSS 4½ x 4½ x 1/8" in the steel tank, the second row columns will be HSS 4½ x 4½ x ¼" in the steel tank, and the third row columns will be HSS 4½ x 4½ x 1/8" in the steel tank. Ultimately, all of the columns will be lined with a 0.25 inch (6.35 mm) 316 Stainless Steel liner to protect against corrosion. Lastly, the columns will be connected to the top plate with a two inch (50.8 mm) thick square plate that is 14 inches (356 mm) wide [10].

The next design element was the bending design for the top plate in each tank, in which the plate was treated as a continuous simply supported plate over the edge of the plate and at the columns, allowing for the use of Timoshenko's method to design the top plate in each tank. Using the annular arrays of columns and normalizing them into rectangular arrays, the moments at the supporting columns for the top plate were calculated using Timoshenko's (1959) theory [15]. Based on Timoshenko, the maximum positive moments, which are the radial moments, occur at the center of the normalized annulus, while the maximum circumferential moment occurs at the halfway point between each column. The maximum negative moment for both directions occurs at the column. Based on the steel plate design, the maximum positive radial moment is 1.040 kip-foot/foot (4.626 kN·m/m), while the maximum negative moment is 1.785 kip-foot/foot (7.940 kN·m/m) [10].

An addition design consideration is that the top plate has a 10 foot (3.048 meter) opening carved out of the plate. This allows for the placement of a removable top dome that will allow pipes into the shell and provide a service access for the tank [10].

For an alternative roof design as shown in Fig. 7, an elliptical carbon steel shell roof with a thickness of 1.5 inches (38.1 mm) is used instead of a flat roof presented in the traditional design. In this design, the elliptical roof has a height of 12 feet (3.658 meters).

8. Foundation Design

The cylindrical tank has a complete foundation design with the foundation sitting on dense sand. In addition, there is a two-foot (610 mm) layer of sand in

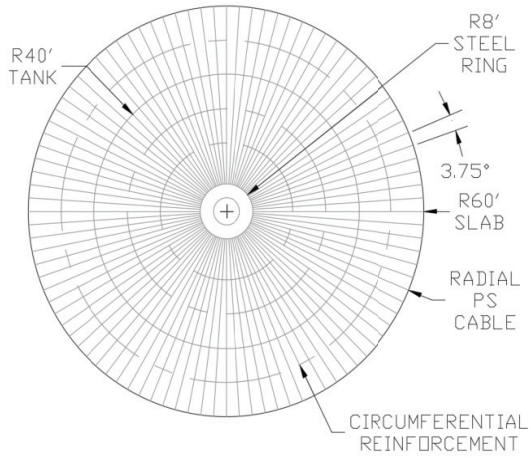

Fig. 8 Posttensioning cable and circumferential reinforcement layout for the circular concrete slab including inner steel ring [10].

between each foundation and the tank. The concrete mat foundation is being designed to not exceed 90 °C as to prevent evaporation of the water of hydration inside the concrete given the long life of the tank. This is addressed later in a heat transfer analysis.

The circular slab requires a thickness of 50 inches (1.270 meters) [10]. Fig. 8 details the configuration of the radial posttensioning cable layout and the connections to the steel ring, as well as the circumferential reinforcement, for the circular concrete slab. The steel ring is used in the circular slab in order to prevent the posttensioning cables from intersecting each other [10].

9. Circular Foundation Radial Pre-stressing

The radial pre-stressing of the slab was the first structural design element of the circular slab foundation. Eqs. (15)-(18) are used to determine the required slab pre-stressing [10].

$$M_{rm} = \frac{kqR^2}{6\phi} \tag{15}$$

$$d_{min} = \sqrt{\frac{M_{rm}}{\omega_p \, f_c^{'} \left(1 - 0.5\omega_p\right)}} \tag{16}$$

$$f_{ps} = f_{py}\left(1 - 0.5\omega_p\right) \tag{17}$$

$$A_{ps} = \frac{2\pi a M_{rm}}{f_{ps} \, d \, (1 - 0.5\omega_p)} \tag{18}$$

According to Timoshenko [15], the maximum radial moment (M_{rm}) at the edge of the tank in Eq. (25) is 1,688.653 kip-foot/foot (7,512 kN-m/m). The slab radius (R) is 60 feet (18.288 meters) and the support condition factor (k) is 0.410.

The design load (q) is 6,178 psf (295.8 kPa) while the bending phi factor (ϕ) is 0.9 as specified in ACI 318-14. The minimum depth (d_{min}) is determined with Eq. (26) using the compressive strength of concrete ($f_c^{'}$), which is 6,000 psi (41.4 MPa), the steel ratio (ω_p), and the maximum radial moment. According to ACI 318-14, the maximum steel ratio is 0.27 for 6,000 psi concrete. In this design, ω_p is 0.21. For the foundation, the required depth for the pre-stressing is 38.697 inches (983 mm), so a depth of 38.75 inches (984 mm) is used. The maximum initial pre-stressing (f_{ps}) based on Eq. (27) is 241.65 ksi (1,666.1 MPa). The required area of all pre-stressing strands (A_{ps}) from Eq. (28) is 911.5 square inches (0.588 square meters) [10].

A negative value corresponds to a positive eccentricity and vice versa. This is done to show the cable path.

Based on this information, the circular foundation will require 96 radial posttensioning 55/0.5 WG cables, which will connect to a steel ring as shown in Fig. 9. Ultimately, the pre-stressing provides a pre-stressing force of 221,760 kips (986,438 kN) in the slab. This is a force of 2,310 kips (10,275 kN) per cable, which causes a pre-stressing stress of 241.379 ksi (1,664.3 MPa) in each cable. At the edge of the circular foundation, the minimum depth of the posttensioning cables is 12.75 inches (324 mm), while the maximum depth of the cables is 38.75 inches (984 mm). Between the edge of the foundation and the edge of the tank, the cables follow a parabolic path as shown in Fig. 9.

10. Circular Foundation Circumferential Reinforcement

The circumferential reinforcement was the next structural design element of the circular slab

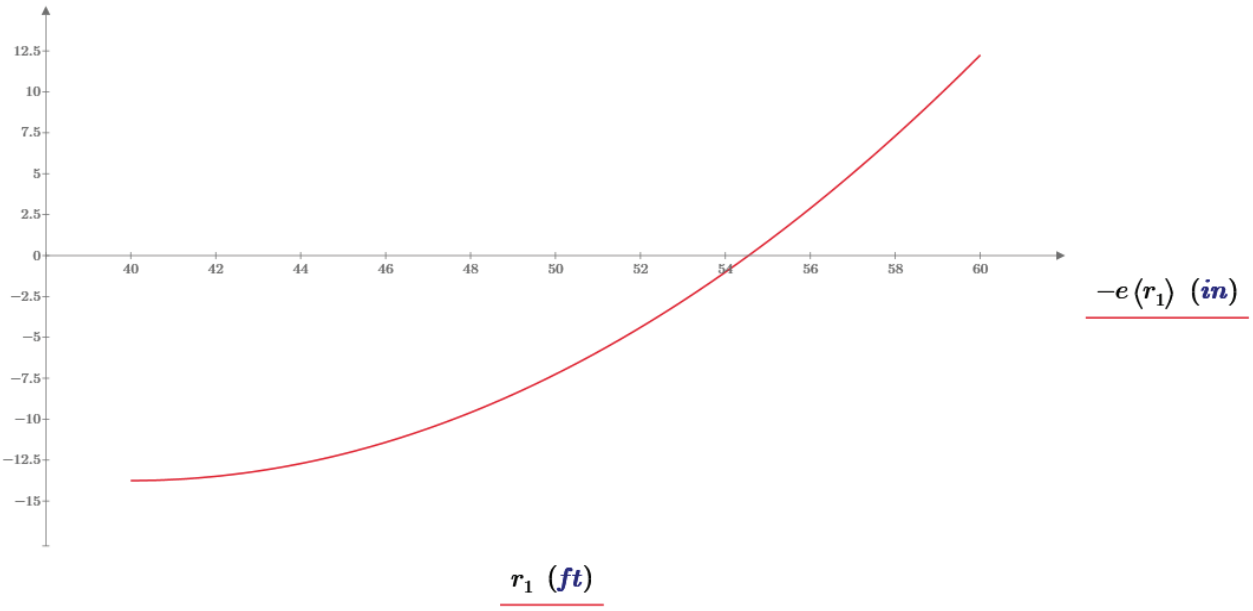

Fig. 9 Inverted eccentricity for the circular slab [10].

foundation. Eqs. (19)-(22) are used to determine the required circumferential reinforcement of the slab [10].

$$M_{cm} = M_{rm}\left(\frac{(3-v_c)R^2-(1+3v_c)r^2}{(3-v_c)R^2-(3-v_c)r^2}\right) \quad (19)$$

$$c = \frac{d\,\varepsilon_c}{\varepsilon_s+\varepsilon_c} \quad (20)$$

$$a = 0.8c \quad (21)$$

$$A_s = \frac{0.85f_c'\,a}{f_y} \quad (22)$$

Based on Timoshenko [15], the maximum circumferential moment (M_{cm}) in Eq. (19) is 2,364.1 kip-foot/foot (10,516 kN·m/m) using a Poission's ratio (v_c) of 0.2 for concrete. The radius of the tank (r) is 40 feet (12.192 meters), while the radius of the circular foundation is 60 feet (18.288 meters).

The required circumferential reinforcement depth is 42.636 inches (1.083 meters) at the edge of the tank. For this design, all of the circumferential reinforcement is located at a depth of 44.125 inches (1.121 meters). The depth of the neutral axis (c) is determined in Eq. (20), which is 16.547 inches (420 mm). The maximum steel strain (ε_s) is 0.005, while the maximum concrete strain (ε_c) is 0.003. The resulting depth of the compression block (a) in Eq. (21) is 13.238 inches (336 mm). The resulting cross-sectional area of steel per foot (A_s) in Eq. (32) is 13.502 square inches (0.009 square meters). As shown in Fig. 10, this results in six #14 Grade 60 reinforcement bars per linear foot [10].

11. Steel Ring for the Circular Foundation

The steel ring connecting the pre-stressing together is the last structural design element for the circular slab foundation. Shown in Fig. 11, the steel ring has an eight foot (2.438 meter) radius, which is r_r in Eqs. (23) and (24).

Eqs. (23)-(25) are used to determine the force in the ring as well as the size of the ring [12].

$$q_r = \frac{P}{2\pi r_r} \quad (23)$$

$$T = q_r r_r \quad (24)$$

$$A = \frac{T}{f_a} \quad (25)$$

The total pre-stressing load (P) on the ring is 221,760 kips (986,438 kN), which results in a uniform ring loading (q_r) of 4,411.8 kips/foot (64,385 kN/m). This produces a ring tensile force (T) of 35,294 kips (156,996 kN). The ring was made of Grade 60 carbon steel and using an allowable stress (f_a) of 36 ksi

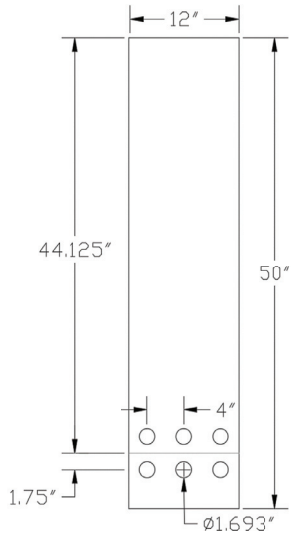

Fig. 10 Circumferential reinforcement layout per foot (Six #14 reinforcement bars per foot) [10].

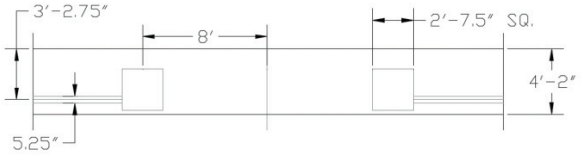

Fig. 11 Layout of the cable and steel ring connection.

(248.211 MPa). The required cross sectional area (A) of the ring is 980.4 square inches (0.633 square meters). For this design, the ring is a square cross-section that is 31.5 inches (800 mm) thick, resulting in a 992.25 square inches (0.640 square meters) cross sectional area [10].

12. Soil Properties Considered in the Foundation Design

When considering the design of granular soils for use in a foundation design, the friction angle must be considered to determine the shear conditions. Tables 4-6 present various results for determining the friction angle from the type of soil and the penetration of the soil. For the design of both foundations presented, dense sand is used.

13. Thermal Expansion of the Cylindrical Tank

The last major consideration for the design of the foundation is to determine the shear stresses between the supporting layer of sand and the bottom of the tank due to thermal expansion of the steel cylindrical tank.

Eq. (26) shows the change in radius due to thermal expansion. Eq. (27) shows the shear stress based on the compression stress exerted on the soil.

$$\Delta R = \alpha R\, \Delta T \tag{26}$$

$$\tau = c + \sigma \tan \phi \tag{27}$$

Based on Eq. (26), ΔR is the change in the radius of the foundation, R is the design radius of the foundation, α is thermal expansion coefficient of steel (13×10^{-6} °C^{-1}), and ΔT is the change in temperature of the steel, which is 560 degrees Celsius [16]. Ultimately, this results in the radius of the tank expanding by 3.493 inches (88.7 mm).

Table 4 Empirical values for f, of granular soils based on the standard penetration number (from Bowels, *Foundation Analysis*) [17].

SPT Penetration N-Value (blows/foot)	f (degrees)
0	25-30
4	27-32
10	30-35
30	35-40
50	38-43

Table 5 Relationship between f, and standard penetration number for sands (from Peck 1974, *Foundation Engineering Handbook*) [17].

SPT Penetration N-Value (blows/foot)	Density of sand	f (degrees)
< 4	Very loose	< 29
4-10	Loose	29-30
10-30	Medium	30-36
30-50	Dense	36-41
> 50	Very dense	> 41

Table 6 Relationship between f, and standard penetration number for sands (from Meyerhof 1956, *Foundation Engineering Handbook*) [17].

SPT Penetration N-Value (blows/foot)	Density of Sand	f (degrees)
< 4	Very loose	< 30
4-10	Loose	30-35
10-30	Medium	35-40
30-50	Dense	40-45
> 50	Very dense	> 45

Based on Eq. (27), τ is the shear stress, σ is the compressive stress, c is the cohesion, and ϕ is the angle of internal friction in the soil. The compressive stress of the soil, which is equal to the weight of the tank and molten salt divided by the area of its base above the foundation, is 5,017 psf (240.2 kPa). The cohesion in the soil is five percent of the bearing stress (6,000 psf), so this results in a cohesion value of 300 psf. Using an angle of internal friction of 35 degrees for loose and coarse sand, the shear stress due to thermal expansion is 3,813 psf (182.6 kPa). Should the coarse sand get compacted with time under the tank load, an angle of internal friction could rise to 45 degrees which results in a maximum shear stress 5,317 psf (254.6 kPa). The shear stress produced by the sand layer is 36.926 psi at which the soil will shear under the bottom of the tank, which is negligible compared to the shear strength of the steel bottom (21.6 ksi) or the concrete foundation (348.6 psi).

The thermal conductivity of quartz sand at 250 °C is 0.31 W/m-K and 0.48 W/m-K at 560 °C, with a closely linear variation in between [18].

In conclusion, the sand layer will allow for an unimpeded expansion of the molten salt tank without any damage to either the bottom of the tank or the concrete foundation.

14. Initial Heat Transfer Analysis

The following are the initial considerations used for the heat transfer analysis used in the molten salt tank structure design. A full and more extensive analytical and numerical solution is beyond the scope of this paper, however, they will appear in a separate future publication. Based on the experimental molten salt storage tank developed at NREL by Halotechnics, Jonemann [19], the maximum observed heat flux for the system was 300 Watts per square meter (W/m^2). Given the fact that the experimental investigation was for a small molten salt tank, our design uses an initial maximum heat flux of 250 W/m^2. Therefore, given that the life of the molten salt storage facility was set for 50 years, a steady state will be achieved in time, which justifies the use of the equations shown below in the analysis and the design of the MS shell. Once an extensive analysis is published, the heat flux may vary somewhat from the initial design presented in this paper.

As stated earlier, two different tank designs were shown in Figs. 6 and 7. In Fig. 6, the steel cylindrical tanks is shown with a flat roof design, while Fig. 7 shows the steel tank with an elliptical roof. Outlining the outside of the shell wall for the steel tank is Kaowool, which is commercially available on Amazon [20]. For the flat roof tank configuration, Kaowool insulation is supported by the columns directly below the roof. When the steel tank has an elliptical roof, the Kaowool insulation is hanging from the roof directly above the shell walls. In addition, the bottom of the tank will contain G-23 firebrick insulation, which is grouted with hot well concrete and placed between the stainless steel layer and the carbon steel layer. Thermal conductivities values for these materials are shown in Table 7 [19, 21].

The first step in performing a heat transfer analysis is to determine the thermal conductivity through the bottom of the tank. Traditional linear thermal conductivity, which is shown in Eq. (28), is used to determine the heat dissipation through the insulating firebrick at the bottom of the tank, which is incased with 0.25 inches (6.35 mm) of stainless steel and 1.5 inches (38.1 mm) of carbon steel [11]. From the bottom of the tank onward, the ground can be treated as a semi-infinite medium, requiring the use of Eq. (29) to describe its behavior over time [22]. In determining this behavior, the temperature of the ground (T_0) is set

Table 7 Thermal conductivity values of insulating and structural material used in tank design [18, 19, 21].

Material	Thermal conductivity (W/m^2)
Kaowool	0.12
Granular Sand	0.40
Carbon Steel	16.0
Stainless Steel	43.0
G-23 Firebrick	0.33

to 15 °C, while the temperature of the salt (T_s) is set to 565 °C. As stated earlier, the life span is 50 years, which is used as the time (t) in Eq. (29). Lastly, the depth of the sand layer (x) between the tank and the supporting concrete slab is 36 inches (914 mm).

$$q = kA\frac{dT}{dx} \tag{28}$$

$$\frac{T(x,t) - T_0}{T_s - T_0} = \text{erf}\left(\frac{x}{2\sqrt{\alpha t}}\right) \tag{29}$$

Based on these equations, the required thickness of firebrick insulation that would allow the concrete slab to stay below 90 °C for the lifespan of the tank is 25 inches (635 mm). The reason for keeping the concrete mat foundation at this temperature is to prevent cracking due to evaporation of the water of hydration inside the concrete given the long life of the tank.

The next step in performing a heat transfer analysis is to determine how heat dissipates through the side walls. This behavior exhibits radial heat conduction, which is detailed in Eq. (28) [11].

$$q = 2\pi krL\frac{dT}{dr} \tag{30}$$

Using Eq. (28), an insulation design was performed for the steel shell tank using the structural shell thicknesses as stated earlier. For the steel tank, 12 inches (305 mm) of Kaowool insulation along the outside of the tank are required to satisfy the maximum flux requirement.

The last step in the heat transfer analysis is determining the heat dissipation through the top of the tank. Eqs. (28) and (31)-(33) are used to describe this behavior [11]. Eq. (31) is used to calculate the flux due to free convection. Eq. (32) is used in calculating the coefficient of convection for the convection pocket immediately above the molten salt. Eq. (33) is used in calculating the coefficient of convection for the convection pocket immediately below the elliptical roof.

$$q = h\,\Delta T \tag{31}$$

$$h = 1.52\sqrt[3]{\Delta T} \tag{32}$$

$$h = 1.31\sqrt[3]{\Delta T} \tag{33}$$

Based on Eqs. (28) and (31)-(33), the thickness of Kaowool insulation can be determined by using the maximum allowed flux of 250 W/m^2. The tank in a flat roof configuration requires 10 inches (254 mm) of Kaowool insulation below the roof. The tank using an elliptical roof requires nine inches (229 mm) of Kaowool insulation.

15. Solar Salt Containment and Safety

Molten nitrate salts tend to wick vigorously and are thus hard to contain. Generally, all pipe joints must be welded, as flanges always leak. However, pump connections are flanged to allow quick pump replacement when necessary. Pumps are, however, typically hung from the tank roofs and thus any flange leakage drips directly back to the tanks.

While valves can theoretically be fully welded using bellows seals, bellows will crack if accidentally operated with frozen salt. Thus, a more traditional valve packing approach is now preferred and is reasonably reliable at cold salt temperatures. Carbon-fiber-impregnated Teflon is usually used as the valve packing material for cold salt valves, although packing nuts must be tightened periodically and packing material must be replaced on an annual basis. There is no practical packing material that can survive at 565 ºC hot salt temperatures for long periods of time, so hot valves typically have "extended bonnets" that, with natural heat loss, can be heat traced to cold salt temperatures. Similar care must be taken with instrumentation installation (e.g., welded thermowells for thermocouples and packing similar to valves for other instrumentation). Note that small leaks from valve stems and instrumentation are not necessarily a serious problem; the salt freezes as it drips and can be knocked loose and returned to the cold tank manually.

Salt containment is another of the primary issues with using salt as the working fluid in troughs. Because the troughs must track the sun, flexible connections are required at the trough ends. Although

sealed bellows were used in early trough systems, they had the problems of failing catastrophically (with associated major leaks) and very high pressure drop. Troughs now use rotating ball joints between trough sections in order to address these problems by using an oil working fluid. However, oils are totally unsuitable for salt because of leakage and freezing of the leaked salt can prevent motion [2].

Any fluid operating at the temperatures of a concentrating solar power (CSP) molten salt system has the inherent danger associated with hot material. In addition, nitrate salts are aggressive oxidizers. While not combustible, they will support combustion of organic materials, necessitating good site cleanliness such as the removal of combustibles such as wooden pallets, paper, and oils. Sandia recommends wearing some sort of fire suit for staff working in close proximity to pressurized salt systems with potential for leakage such as the steam generator system with its many valves and connections, although this precaution is generally not necessary in all areas of the plant.

From an environmental perspective, nitrate salts are essentially fertilizers, so small releases are not a major concern. In addition, salt leaks and minor spills will freeze quickly and before migrating into the surrounding environment. In this regard, cleanup is relatively simple, picking up the frozen salt and returning it to the tanks to re-melt. However, nitrate salts are highly soluble in water, so rain can spread the material if not cleaned up in a timely fashion. Note that berming is required around the storage tanks, to contain the salt in the extremely unlikely event of a major tank leak or rupture. One idea to help in the cleanup process is to construct a steel side wall around any molten salt tank in order to contain the salts and prevent human contact from molten salts immediately after an incident [1, 2].

Martin Marietta [23] conducted a major study of MS safety study in 1980, and Sandia has developed safe operating procedures for MS operations.

16. Conclusions

In designing molten salt storage tanks, the most important design considerations are the structural design, insulation, and foundations. Funding for this research came from the Office of Naval Research (ONR).

References

[1] Ladkany, S., Culbreth, W., and Loyd, N. 2016. "Characteristics of Molten Salts and Recommendations for Use in Solar Power Stations." ISEC Press.

[2] Tyner, C. 2015. "Concentrating Solar Power and Molten Salt Energy Storage Systems Background, Survey Report Presented to Molten Salt Project at UNLV." Tyner Consulting.

[3] Ladkany, S., Culbreth, W., and Loyd, N. 2018. "Molten Salt History, Types, Thermodynamic and Physical Properties, and Cost." *Journal of Energy and Power Engineering*. David Publishing Company.

[4] Ladkany, S., Culbreth, W., and Loyd, N. 2018. "Worldwide Molten Salt Technology Developments in Energy Production and Storage." *Journal of Energy and Power Engineering*. David Publishing Company.

[5] "Optimal Design of a Molten Salt Thermal Storage Tank for Parabolic Trough Solar Power Plants."

[6] Bradshaw, R. W., and Goods, S. H. 2001. "Corrosion Resistance of Stainless Steels during Thermal Cycling in Alkali Nitrate Molten Salts." Sandia National Laboratory.

[7] Sohal, M., Ebner, M., Sabharwall, P., and Sharpe, P. 2010. "Engineering Database of Liquid Salt Thermophysical and Thermochemical Properties." Idaho National Laboratory. Retrieved from http://www.inl.gov/technicalpublications/Documents/4502650.pdf on Feb. 6, 2015.

[8] Kelly, B. 2000. Lessons Learned, Project History, and Operating Experience of the Solar Two Project, Sandia National Laboratories Report, SAND2000-2598.

[9] Raade, J., Roark, T., Vaughn, J., and Bradshaw, R. 2013. Deep Eutectic Salt Formulations Suitable as Advanced Heat Transfer Fluids, Halotechnics Report DE-FG36-08GO18144.

[10] Loyd, N. 2016. "Solar Energy Storage in Molten Salt Shell Structures." University of Nevada, Las Vegas.

[11] Holman, J. P. 1986. *Heat Transfer*, 6th ed. New York, NY: McGraw-Hill.

[12] Urugal, A. C. 2009. *Theory of Beams, Plates, and Shells*. 4th ed. Boca Raton, FL: CRC Press.

[13] Salmon, C. G., Johnson, J. E., and Malhas, F. A. 2009. *Steel Structures: Design and Behavior*. 5th ed. Upper

Saddle River, NJ: Pearson Prentice Hall.

[14] *Steel Construction Manual*. 14th ed. American Institute of Steel Construction, 2012.

[15] Timoshenko, S. 1959. *Theory of Plates and Shells*. New York: McGraw-Hill.

[16] Angle of Internal Friction. Geotechnical Info, 2012. Retrieved from http://www.geotechnicalinfo.com/angle_of_internal_friction.html on May 20, 2016.

[17] Thermal Expansion Coefficients at 20 C. HyperPhysics. Retrieved from http://hyperphysics.phy-astr.gsu.edu/hbase/tables/thexp.html on May 20, 2016.

[18] Bauman, T., and Zunft, S. 2011. "Properties of Granular Materials for Use as Heat Transfer Media for a Moving Bed Heat Exchanger in CSP Application." Retrieved from https://elib.dlr.de/71021/1/ECCE_2011_engl_22_09.pdf.

[19] Jonemann, M. 2013. Advanced Thermal Storage System with Novel Molten Salt, National Renewable Energy Laboratory Report, NREL/SR-5200-58595.

[20] "CM-Ceramics 1." Ceramic Fiber Insulation Blanket". Amazon. Retrieved from https://www.amazon.com/CM-Ceramics-Insulation-Ceramics-Material-Instructions/dp/B00GT5Q6X0/ref=sr_1_1_sspa/131-9226715-2000562?ie=UTF8&qid=1542671848&sr=8-1-spons&keywords=kaowool&psc=1.

[21] "Thermal Conductivity of common Materials and Gases." 2003. Engineering ToolBox. Retrieved from https://www.engineeringtoolbox.com/thermal-conductivity-d_429.html.

[22] "Unsteady Heat Transfer in Semi-infinite Solids." Florida State University. Retrieved from http://www.eng.fsu.edu/~shih/eml3016/lecture-notes/semi-infinite.ppt.

[23] Marietta, M. 1980. Molten Salt Safety Study, Sandia National Laboratories Report, SAND80-8179.